Materials Transactions, Vol. 44, No. 9 (2003) pp. 1885 to 1890
©2003 The Japan Institute of Metals
EXPRESS REGULAR ARTICLE

Hydrogen Permeation Characteristics of Melt-Spun Ni–Nb–Zr Amorphous Alloy Membranes

Shin-ichi Yamaura[1,*], Yoichiro Shimpo[2], Hitoshi Okouchi[2], Motonori Nishida[2], Osamu Kajita[2], Hisamichi Kimura[1] and Akihisa Inoue[1]

[1]*Institute for Materials Research, Tohoku University, Sendai 980-8577, Japan*
[2]*Fukuda Metal Foil & Powder Co. Ltd., Kyoto 607-8305, Japan*

We prepared the melt-spun $(Ni_{0.6}Nb_{0.4})_{100-x}Zr_x$ ($x = 0$ to 40 at%) and other amorphous alloy membranes and examined the permeation of hydrogen through those alloy membranes. The interatomic spacing in the Ni–Nb–Zr amorphous structure increased with increasing Zr content. The crystallization temperature of the Ni–Nb–Zr amorphous alloys decreased with increasing Zr content. The hydrogen flow increased with an increase of the temperature or the difference in the square-roots of hydrogen pressures across the membrane, $\Delta\sqrt{p}$. At relatively higher temperature up to 673 K or at relatively higher hydrogen pressure difference, $\Delta\sqrt{p}$ up to 550 $Pa^{1/2}$, the hydrogen flow was more strictly proportional to $\Delta\sqrt{p}$. This indicates that the diffusion of hydrogen through the membrane is a rate-controlling factor for hydrogen permeation. The permeability of the Ni–Nb–Zr amorphous alloys was strongly dependent on alloy compositions and increased with increasing Zr content. However, it was difficult to investigate the hydrogen permeability of the $(Ni_{0.6}Nb_{0.4})_{60}Zr_{40}$ amorphous alloy in this work due to the embrittlement during the measurement. The maximum hydrogen permeability was 1.3×10^{-8} ($mol \cdot m^{-1} \cdot s^{-1} \cdot Pa^{-1/2}$) at 673 K for the $(Ni_{0.6}Nb_{0.4})_{70}Zr_{30}$ amorphous alloy. It is noticed that the hydrogen permeability of the $(Ni_{0.6}Nb_{0.4})_{70}Zr_{30}$ amorphous alloy is higher than that of pure Pd metal. These permeation characteristics indicate the possibility of future practical use of the melt-spun amorphous alloys as a hydrogen permeable membrane.

(Received July 9, 2003; Accepted August 11, 2003)

Keywords: *hydrogen permeation, hydrogen separation, amorphous alloy, melt-spinning*

1. Introduction

Recently, the conversion of the fossil-fuel consuming society to the hydrogen powered society is strongly required all over the world in the viewpoint of the suppression of global warming. A great number of researchers and engineers have been working for the development of many types of high-performance fuel cells in the world.[1–5] In order to use fuel cells practically in our everyday life in future, much more improvement of the total performance of fuel cells such as high power, long lifetime and low running cost is required. Furthermore, a stable hydrogen supply will also be an essential factor to use fuel cells in our life. There are many production techniques of pure hydrogen.[6–13] For instance, we can obtain pure hydrogen gas by using the fossil-fuel reforming[6–8] or the water electrolysis.[9–11] In case of using the fossil-fuel reforming when producing gaseous hydrogen, purification of hydrogen by the hydrogen permeable membrane in the final process of hydrogen production will be required because hydrogen gas produced by the reforming reaction includes a large amount of byproduct gases such as CO as contamination that cause significant degradation of the fuel cells.[14] The mechanism of purification of hydrogen gas by using a hydrogen permeable membrane is very simple, cost-saving and suitable for continuous production.[15] Therefore, if the membrane process is widely used for producing high-purity hydrogen, mass-production of pure hydrogen at relatively low cost will become available in future.

Nowadays, there are three types of hydrogen permeable membranes. They are a polymer membrane,[16] a porous ceramics membrane[17] and a metallic membrane.[18] In particular, a metallic membrane is the most preferable one among these types of membranes because of its excellent hydrogen selectivity and high thermal stability. In fact, the Pd–Ag alloy membranes have been practically used for hydrogen purification for decades especially in the field of semiconductor industries and nuclear fusion engineering.[19,20] However, since the Pd metal is extremely expensive, it is very important to search for a new alloy which can replace the Pd–Ag alloys as hydrogen permeable membrane materials. The new alloy must be non-Pd-based alloys with the minimum Pd addition. As for the non-Pd-based membrane alloys, it was reported that the V–Ni alloys[21] possessed excellent hydrogen permeability which is nearly the same as that of the Pd–Ag alloys, though hydrogen embrittlement of the alloy is significant. The requirements which the hydrogen permeable membranes have to satisfy are not only high hydrogen permeability (high hydrogen solubility and high hydrogen diffusivity) but also excellent immunity from hydrogen embrittlement.[21] Hydrogen embrittlement is known to be one of the most important subjects of iron and steel industries for a long time.[22] Therefore, hydrogen permeable metallic membranes also cannot escape hydrogen embrittlement.

Amorphous alloys are known to possess higher mechanical strength[23] than crystalline ones and relatively strong immunity from hydrogen embrittlement due to high hydrogen solubility.[24] In order to employ these characteristic properties of amorphous alloys in the development of new hydrogen permeable membranes,[25–28] Sakaguchi *et al.* and Adachi *et al.* studied hydrogen permeability and hydrogen embrittlement of amorphous thin films of $LaNi_5$ hydrogen storage alloy.[29,30] Moreover, Hara *et al.* studied hydrogen permeability and embrittlement of melt-spun amorphous Ni–Zr and Ni–M–Zr (M = Ti and Hf) alloys and reported that these alloys had enough mechanical strength without suffering

*Corresponding author, E-mail: yamaura@imr.tohoku.ac.jp

from embrittlement although those hydrogen permeability was much lower than that of the Pd–Ag alloys.[31,32] We have tried to develop a practical membrane with high hydrogen permeability without hydrogen-induced embrittlement by employing Ni-based amorphous alloy as a membrane material on the basis of some previous data that the amorphous Ni–Zr alloys exhibit useful properties such as high efficient catalytic characteristics for carbon monoxide,[33] hydrogenation of benzene[34] and hydrogen permeation.[31] Furthermore, it is expected that the Nb addition improves the performance of amorphous membrane because the permeability of Nb metal is higher than that of the Pd–Ag alloys. The bulk glassy alloys have been found in Mg-[35] and Lanthanide (Ln)-[36] systems in 1988 and 1989, respectively, and then widely extended to even Ni-based alloys.[37,38] Recently, Inoue *et al.* have found that Ni-based bulk glassy alloys with a large supercooled liquid region before crystallization are formed in Ni–Nb–Ti–Zr system.[39] Subsequently, Kimura *et al.* have studied the glass-forming ability of Ni–Nb–Zr system and reported that glassy or amorphous Ni–Nb–Zr alloys could be produced in a wide composition range by melt-spinning.[40] The objective of this work is to produce amorphous Ni-based alloys (especially Ni–Nb–Zr alloys) by the melt-spinning technique and to examine the hydrogen permeability of the alloys.

2. Experimental

$(Ni_{0.6}Nb_{0.4})_{100-x}Zr_x$ ($x = 0$, 20, 30 and 40 at%), $Ni_{45}Nb_{45}Zr_{10}$, $Ni_{65}Nb_{25}Zr_{10}$ and $Ni_{44}Nb_{43}Zr_{10}Pd_3$ alloy ingots were prepared by arc-melting the mixture of pure metals in an Ar atmosphere. Melt-spun ribbons were produced by the single-roller melt-spinning technique in an Ar atmosphere. The ribbons were about 20 mm wide and 30–40 μm thick. The amorphicity of melt-spun ribbon specimens was investigated by X-ray diffractometry (CuKα, 40 kV, 30 mA, hereafter denoted as XRD). Thermal stability of melt-spun ribbon specimens was examined by differential scanning calorimetry (DSC) at a heating rate of 0.67 K s^{-1} in an Ar atmosphere. Pd thin film was deposited on both sides of specimens by the sputtering technique as an active catalyst for hydrogen dissociation and recombination during permeation. Hydrogen permeation measurements were performed with a conventional gas-permeation technique in the temperature range of 573 to 673 K at the hydrogen pressure up to 0.7 MPa. Sample membranes were mounted in the gas-permeation cell. The diameter of the permeation area was 10 mm. Pure hydrogen gas was introduced to one side of a membrane and then the flow rate of effluent hydrogen gas from the other side (permeate side) was measured by the mass flow meter.

3. Results and Discussion

Figure 1 shows the XRD patterns of the melt-spun $(Ni_{0.6}Nb_{0.4})_{100-x}Zr_x$ ($x = 0$, 20, 30 and 40 at%) alloy ribbons. No sharp diffraction peaks are observed in the 2θ range of 20–80°. This indicates that all alloys possess a single amorphous phase. Besides, a halo peak shifts to lower angles with increasing Zr content, indicating that the interatomic spacing in the amorphous structure increases by the addition of Zr. All other alloys prepared in this study were also confirmed to have a single amorphous phase.

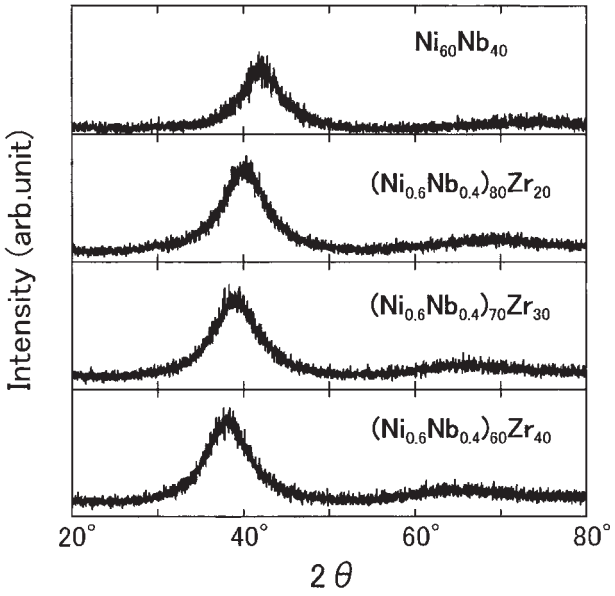

Fig. 1 XRD patterns of melt-spun $(Ni_{0.6}Nb_{0.4})_{100-x}Zr_x$ ($x = 0$, 20, 30 and 40 at%) alloys.

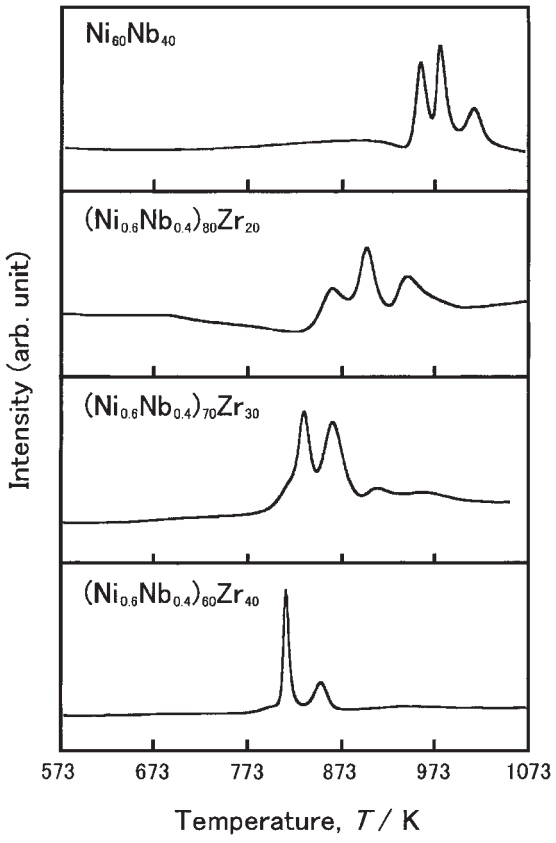

Fig. 2 DSC curves of melt-spun $(Ni_{0.6}Nb_{0.4})_{100-x}Zr_x$ ($x = 0$, 20, 30 and 40 at%) alloys.

Figure 2 shows the DSC curves of the $(Ni_{0.6}Nb_{0.4})_{100-x}Zr_x$ ($x = 0$, 20, 30 and 40) amorphous alloys. The crystallization temperatures of the $(Ni_{0.6}Nb_{0.4})_{100-x}Zr_x$ ($x = 0$, 20, 30 and 40 at%) alloys are 946 K, 837 K, 794 K and 777 K, respec-

tively, and decrease with increasing Zr content. The maximum temperature at which hydrogen permeation was measured in this work was 673 K which was lower by more than 100 K than the crystallization temperature. Kimura *et al.* studied the amorphous formability of the Ni–Nb–Zr ternary alloys and reported that the $Ni_{60}Nb_{20}Zr_{20}$ glassy alloy possessed a large supercooled liquid region, ΔT_x ($= T_x - T_g$, T_x: crystallization temperature, T_g: glass transition temperature) of 51 K.[40] However, the amorphous alloys prepared in this work possess much narrower or no supercooled liquid region as shown in Fig. 2. It is an interesting subject to study the relationship between the hydrogen permeation and the compositional range with a wide supercooled liquid region in the Ni–Nb–Zr ternary system. However, the compositional range of the Ni–Nb–Zr alloys possessing a wide supercooled liquid region is limited within $10 < Nb < 30$, $10 < Zr < 40$ and $50 < Ni < 70$ at%. In this work, we prepared the Ni–Nb–Zr alloys with higher concentrations of Nb and Zr elements because of their strong affinity with hydrogen.

In general, the permeation of hydrogen through a membrane is thought to occur through the following three steps; 1) the dissociation of hydrogen gaseous molecules into hydrogen atoms on the surface of the upper side of the membrane, 2) the diffusion of hydrogen atoms through the membrane, and 3) the recombination of hydrogen atoms on the surface of the permeate side of the membrane. When the hydrogen behavior is interpreted on the basis of the above mentioned mechanism, the hydrogen permeation rate F ($\mathrm{mol \cdot m^{-2} \cdot s^{-1}}$) can be estimated by the following equation;

$$F = \frac{P}{d}\left(\sqrt{p_1} - \sqrt{p_2}\right) = \frac{P}{d} \cdot \Delta\sqrt{p},$$

where P is the hydrogen permeability ($\mathrm{mol \cdot m^{-1} \cdot s^{-1} \cdot Pa^{-1/2}}$) and d is the membrane thickness (m). And p_1 and p_2 are the hydrogen pressures of the upper side and of the permeate side of the membrane (Pa), respectively. In case that measured hydrogen permeation rate is proportional to $\Delta\sqrt{p}$, the hydrogen diffusion is regarded as the rate-controlling factor for hydrogen permeation of the membrane.

Figure 3 shows the hydrogen permeation rates of the amorphous $Ni_{60}Nb_{40}$, $(Ni_{0.6}Nb_{0.4})_{80}Zr_{20}$ and $(Ni_{0.6}Nb_{0.4})_{70}Zr_{30}$ alloys as a function of the difference in square roots of the hydrogen pressures between the upper side and the permeate side of the membrane, $\Delta\sqrt{p}$. In Fig. 3(a), although the hydrogen permeation rate is almost proportional to $\Delta\sqrt{p}$, the plot does not cross the origin of the coordinate axes. This is probably because the hydrogen flow through $Ni_{60}Nb_{40}$ is too small to measure accurately by a mass flow meter used in this work. On the contrary, as the amount of permeated hydrogen increases with increasing $\Delta\sqrt{p}$, the proportionality of the hydrogen flow as a function of $\Delta\sqrt{p}$ increases as shown in Figs. 3(b) and (c). However, as shown in Fig. 3(c), the hydrogen flow is not always proportional to $\Delta\sqrt{p}$ at relatively low pressure difference. This is presumably because the hydrogen pressure is not high enough to activate the dissociation of hydrogen gas to hydrogen atoms on the upper side of the membrane even for the $(Ni_{0.6}Nb_{0.4})_{70}Zr_{30}$ alloy and the rate-controlling factor of hydrogen permeation in such a low pressure region may be surface reactions rather than diffusion inside the alloy. The hydrogen permeation rate of the amorphous $Ni_{60}Nb_{40}$ alloy was about 1.23×10^{-2} ($\mathrm{mol \cdot m^{-2} \cdot s^{-1}}$) even at the hydrogen pressure difference of $\Delta p = 0.39$ MPa ($\Delta\sqrt{p} = 370$; $p_1 = 0.403$ MPa, $p_2 = 0.015$ MPa) at 673 K. The hydrogen permeation rate of the amorphous $(Ni_{0.6}Nb_{0.4})_{70}Zr_{30}$ alloy was about 1.45×10^{-1} ($\mathrm{mol \cdot m^{-2} \cdot s^{-1}}$) at the hydrogen difference of $\Delta p = 0.46$ MPa ($\Delta\sqrt{p} = 391$) and more than 2×10^{-1} ($\mathrm{mol \cdot m^{-2} \cdot s^{-1}}$) at $\Delta p = 0.74$ MPa ($\Delta\sqrt{p} = 548$), being much larger than that of the amorphous $Ni_{60}Nb_{40}$ alloy. It was clearly shown that the hydrogen flow was proportional to $\Delta\sqrt{p}$ at 673 K and the hydrogen diffusion is a rate-controlling factor for hydrogen permeation of this alloy. The hydrogen flow of the $(Ni_{0.6}Nb_{0.4})_{70}Zr_{30}$ amorphous alloy also increased linearly with an increase of $\Delta\sqrt{p}$ in the difference range over $\Delta p = 0.25$ MPa. This result clearly indicates that the mechanism for hydrogen permeation of this alloy is controlled by hydrogen diffusion, as shown in Fig. 3(c). However, the hydrogen flow at relatively smaller pressure difference is smaller than that estimated from the above-described equation presumably because of the low activity to the dissociation of hydrogen gas to hydrogen atoms on the upper side of the membrane as mentioned above. Moreover, since the membranes of the amorphous $(Ni_{0.6}Nb_{0.4})_{60}Zr_{40}$ alloy became brittle during the test, it was difficult to measure the hydrogen permeation of these alloy membranes by the sample holder used in this work.

Figure 4 shows the Arrhenius plots of the hydrogen permeability of all alloys prepared in this work. Plots of Pd–23 mass%Ag and Pd metal are included in the figure. The permeation data of the Pd–23 mass%Ag was also measured in this work and that of the Pd metal was referred to the previous report.[41] The maximum hydrogen permeability is 1.1×10^{-9} ($\mathrm{mol \cdot m^{-1} \cdot s^{-1} \cdot Pa^{-1/2}}$) for the $Ni_{60}Nb_{40}$ amorphous alloy, 6.7×10^{-9} ($\mathrm{mol \cdot m^{-1} \cdot s^{-1} \cdot Pa^{-1/2}}$) for the $(Ni_{0.6}Nb_{0.4})_{80}Zr_{20}$ amorphous alloy and 1.3×10^{-8} ($\mathrm{mol \cdot m^{-1} \cdot s^{-1} \cdot Pa^{-1/2}}$) for the $(Ni_{0.6}Nb_{0.4})_{70}Zr_{30}$ amorphous alloy at 673 K. The hydrogen permeability of the melt-spun amorphous $Ni_{44}Nb_{43}Zr_{10}Pd_3$, $Ni_{45}Nb_{45}Zr_{10}$ and $Ni_{65}Ni_{25}Zr_{10}$ alloys is also shown in Fig. 4. It is shown that the permeability of the $(Ni_{0.6}Nb_{0.4})_{100-x}Zr_x$ ($x = 0$, 20 and 30 at%) alloys increases with increasing Zr content and there is a tendency for permeability to increase with increasing temperature. As seen in Fig. 1 showing the XRD patterns of the melt-spun $(Ni_{0.6}Nb_{0.4})_{100-x}Zr_x$ ($x = 0$, 20, 30 and 40 at%) alloys, a halo peak shifts to a lower angle side with increasing Zr content.

Figure 5 indicates the hydrogen permeability and the wave vector, $K_p = \frac{4\pi \sin\theta}{\lambda}$ as a function of Zr content of the alloys. It is shown that the permeability increases with decreasing the wave vector K_p value. The change in the K_p value indicates that the nearest neighbor distance of the atoms in the amorphous structure increases by Zr addition. It can be said that the amorphous alloy having a larger atomic spacing possesses higher hydrogen permeability in this alloy system. However, there is an optimum Zr content in this alloy system because the Zr addition decreases the thermal stability of their alloys as shown in Fig. 2 and may embrittle those alloys during hydrogen permeation because of a large amount of hydrogen absorption.

We tentatively calculate the activation energy for hydro-

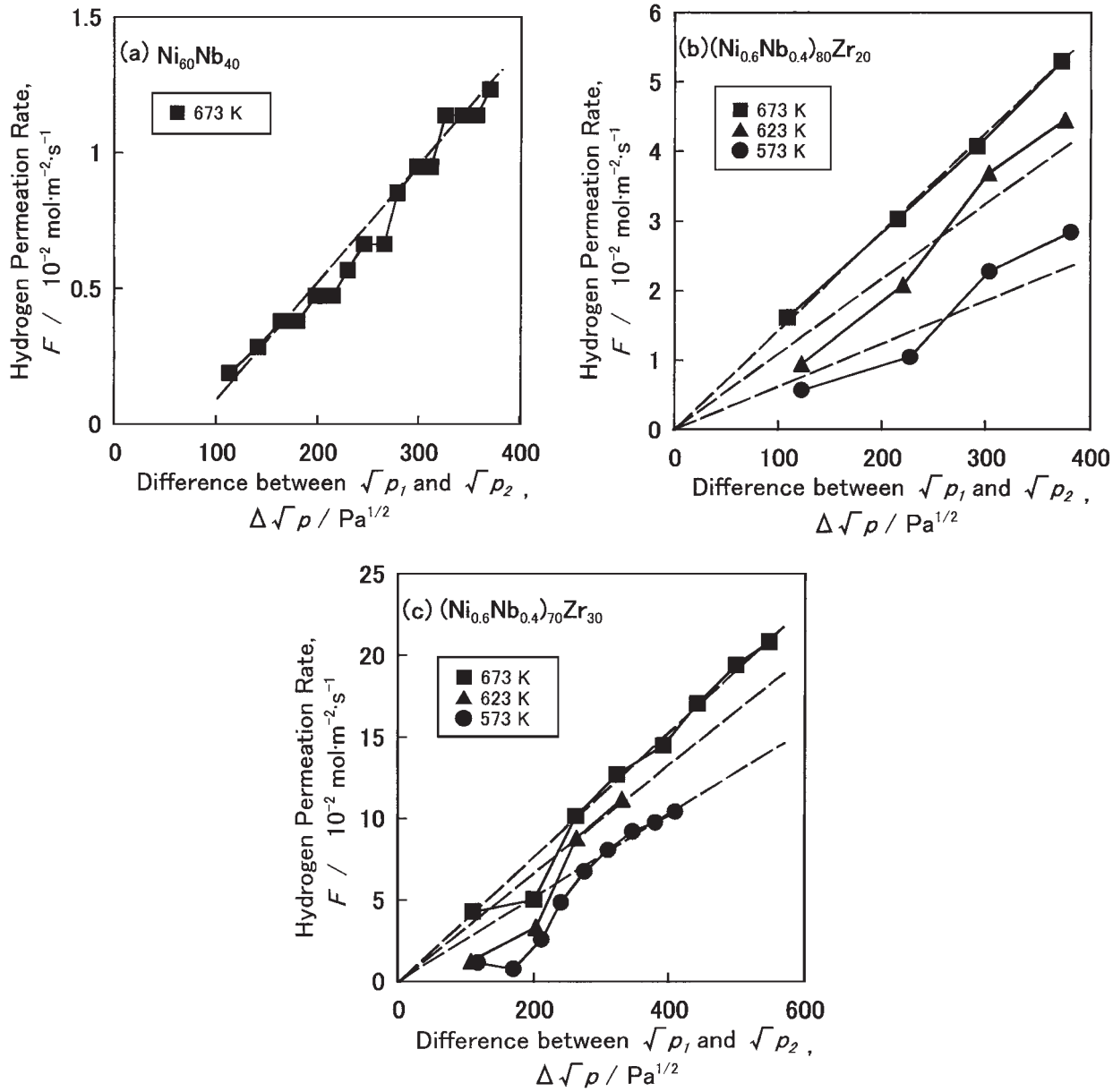

Fig. 3 Hydrogen flow rates of melt-spun amorphous (a) $Ni_{60}Nb_{40}$, (b) $(Ni_{0.6}Nb_{0.4})_{80}Zr_{20}$ and (c) $(Ni_{0.6}Nb_{0.4})_{70}Zr_{30}$ alloys as a function of the difference in square roots of the hydrogen pressure between the upper side and the permeate side of the membrane specimen.

gen permeation of the alloys used in the present work. The activation energy, Q (kJ·mol^{-1}) and the pre-exponential factor, q_0 (mol·m^{-1}·s^{-1}·Pa$^{-1/2}$) are summarized in Table 1. The activation energy for hydrogen permeation of the $(Ni_{0.6}Nb_{0.4})_{70}Zr_{30}$ amorphous alloy is mostly comparable to that of the Pd metal. And the pre-exponential factor, q_0 of the $(Ni_{0.6}Nb_{0.4})_{70}Zr_{30}$ amorphous alloy is much larger than that of the Pd metal. Therefore, it is understandable that the hydrogen permeation of the $(Ni_{0.6}Nb_{0.4})_{70}Zr_{30}$ amorphous alloy is slightly larger than that of the Pd metal. The Pd–23 mass%Ag alloy possesses tremendously small activation energy due to small temperature-dependence of the hydrogen permeation.

Figures 6(a) and (b) indicate the XRD pattern and the DSC curve of the $(Ni_{0.6}Nb_{0.4})_{70}Zr_{30}$ membrane obtained after the hydrogen permeation test. In this permeation test, it took about 2.5 h to heat the specimen up to 673 K and about 1 h to measure the permeability. It is clearly shown in Fig. 6(a) that the membrane specimen can possess a single amorphous phase without any sharp peaks except one peak which comes from Pd surface film even after the permeation test at high temperature and high hydrogen pressure. As shown in Fig. 6(b), two exothermic peaks appear at about 833 K and at about 868 K, respectively. In general, an exothermic crystallization peak of hydrogen absorbed amorphous alloy moves to lower temperature side because the amorphous alloy becomes thermally unstable by hydrogenation. However, peak position of the two peaks does not change comparing DSC curves obtained from the specimens before and after permeation test (for comparison, see Fig. 2). This result suggests that the specimen after permeation test does not contain hydrogen so much. Moreover, the specimen after the permeation test exhibits a wide endothermic region with two broad endothermic peaks presumably due to hydrogen

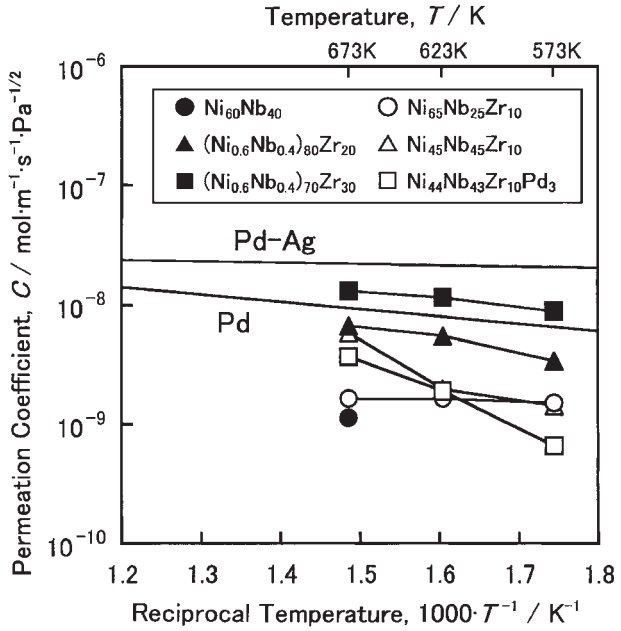

Fig. 4 Arrhenius plots of the hydrogen permeability of all alloys prepared in this work.

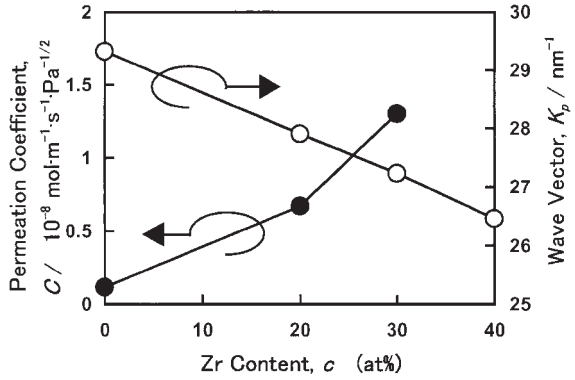

Fig. 5 The hydrogen permeability and the wave vector as a function of Zr content of the alloys.

desorption in the lower temperature range from 573 to 773 K. The origin of this endothermic behavior is not clear at the present time. In this work, the permeation tests were performed at up to 643 K. Since the temperature at which the permeation tests were performed is in the endothermic region, hydrogen atoms may permeate this amorphous alloy membrane without significant hydrogen absorption by the membrane. As mentioned above, the amorphous $(Ni_{0.6}Nb_{0.4})_{60}Zr_{40}$ alloy became brittle during the test. However, such embrittlement may not come from hydrogen-induced embrittlement. If so, why were the amorphous membranes embrittled during the permeation test? The reason is not clear. But one of the present authors (S.Y.) think tentatively that a severe deformation of the membrane especially at around a metal gasket at high temperature and high hydrogen pressure may be harmful because it was reported that the mechanical strength of the Ni–Nb–Zr amorphous alloys decreases with Zr addition and think that this problem may be solved by optimization of the design of a sample holder.

Table 1 The activation energy, Q (kJ·mol^{-1}) and the pre-exponential factor, q_0 (mol·m^{-1}·s^{-1}·Pa$^{-1/2}$) of the $(Ni_{0.6}Nb_{0.4})_{80}Zr_{20}$ and the $(Ni_{0.6}Nb_{0.4})_{70}Zr_{30}$ amorphous alloys. p_1 and p_2 are the hydrogen pressures of the upper side and of the permeate side of the membrane (Pa), respectively.

Composition	Q (kJ·mol^{-1})	q_0 (mol·m^{-1}·s^{-1}·Pa$^{-1/2}$)
$(Ni_{0.6}Nb_{0.4})_{80}Zr_{20}$	22.1	1.3×10^{-7}
$(Ni_{0.6}Nb_{0.4})_{70}Zr_{30}$	12.7	3.6×10^{-7}
Pd–23 mass%Ag	1.7	2.9×10^{-8}
Pd[41]	11.7	7.6×10^{-8}

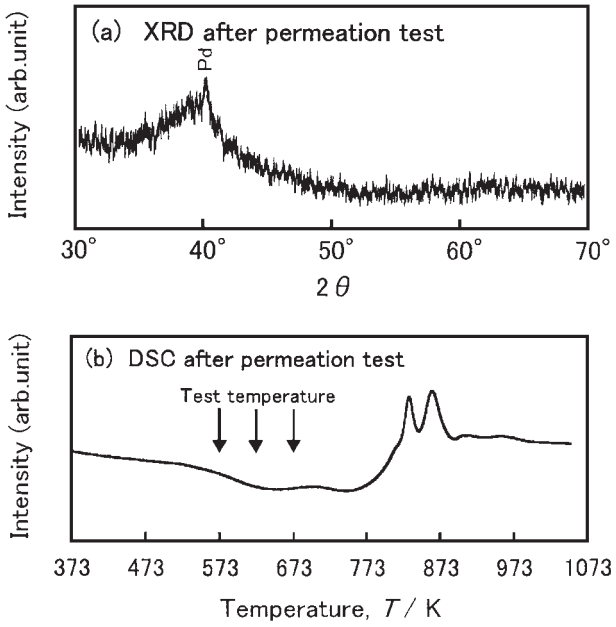

Fig. 6 (a) The XRD pattern and (b) the DSC curve of the $(Ni_{0.6}Nb_{0.4})_{70}Zr_{30}$ amorphous alloy after the hydrogen permeation test.

From these results, it is concluded that the hydrogen permeability of the amorphous Ni–Nb–Zr alloy is sensitive to alloy composition. It is important to investigate an optimum composition in order to improve the hydrogen permeability of the Ni–Nb–Zr alloys. The $(Ni_{0.6}Nb_{0.4})_{70}Zr_{30}$ amorphous alloy shows the highest hydrogen permeability of 1.3×10^{-8} (mol·m^{-1}·s^{-1}·Pa$^{-1/2}$) at 673 K among the alloys studied in this work. The permeability of the alloy is larger than that of pure Pd metal. These results indicate the possibility for future practical use of the amorphous Ni–Nb–Zr alloys having high hydrogen permeability.

4. Conclusions

Hydrogen permeation was examined for the melt-spun amorphous Ni–Nb–Zr alloys. The results obtained are summarized as follows;

(1) The halo peak of the $(Ni_{0.6}Nb_{0.4})_{100-x}Zr_x$ amorphous alloys shifts to a lower angle side with increasing Zr content. The interatomic spacing in their amorphous structure increases with Zr addition. The crystallization temperature of the $(Ni_{0.6}Nb_{0.4})_{100-x}Zr_x$ amorphous alloys decreases with increasing Zr content, showing that the amorphous structure becomes thermally unstable by the Zr addition.

(2) The hydrogen flow increases with increasing temperature or difference in the square-roots of hydrogen pressures of both sides of the membrane, $\Delta\sqrt{p}$. At higher temperature up to 673 K or larger $\Delta\sqrt{p}$ up to 550 $Pa^{1/2}$, the hydrogen flow is more accurately proportional to $\Delta\sqrt{p}$. The diffusion through the membrane is concluded to be a rate-controlling factor for hydrogen permeation. However, the hydrogen flow is not always proportional to $\Delta\sqrt{p}$ at relatively low temperature or at relatively small difference in hydrogen pressures. This is presumably because the hydrogen pressure is not large enough to activate the dissociation of hydrogen gas to hydrogen atoms on the upper side of the membrane and the rate-controlling factor for hydrogen permeation is surface reactions rather than diffusion inside the alloy in such a low hydrogen pressure region.

(3) The permeability of the Ni-based amorphous alloys is strongly dependent on their alloy compositions. The hydrogen permeability of the melt-spun $(Ni_{0.6}Nb_{0.4})_{70}Zr_{30}$ amorphous alloy is 1.3×10^{-8} $(mol/m\,s\,Pa^{1/2})$ at 673 K which is slightly larger than that of pure Pd metal.

(4) The $(Ni_{0.6}Nb_{0.4})_{70}Zr_{30}$ amorphous alloy can possess an amorphous phase even after the permeation test without unstabilization caused by hydrogenation. This may be because the test temperature in this work is in the temperature range at which the desorption of hydrogen can occur.

Acknowledgements

This work was supported by the New Energy and Industrial Technology Development Organization (NEDO) of Japan under the Research program, "Research and Development of Polymer Electrolyte Fuel Cell"

REFERENCES

1) F. T. Bacon: Electrochim. Acta **14** (1969) 569–585.
2) K. Strasser: J. Electrochem. Soc. **127** (1980) 2172–2177.
3) A. F. Sammells, S. B. Nicholson and P. G. P. Ang: J. Electorchem. Soc. **127** (1980) 350–357.
4) N. Q. Minh: J. Amer. Ceram. Soc. **76** (1993) 563–5688.
5) Solid Polymer Electolyte Fuel Cell Technology Program (General Electric Co.), Final Report NASA-CR-160734 (1980).
6) W. Balthasar: Int. J. Hydrogen Energy **9** (1984) 649–668.
7) M. Steinberg and H. C. Cheng: Int. J. Hydrogen Energy **14** (1989) 797–820.
8) Y. Yurum: in Hydrogen Energy System, -Production and Utilization of Hydrogen and Future Aspects, NATO ASI Series Kluwer Academic Publishers **E-Vol.295** (1995) 15–30.
9) H. Wendt and G. Imarisio: J. Appl. Electrochem. **18** (1988) 1–14.
10) P. Millet, F. Andolfatto and R. Durand: Int. J. Hydrogen Energy **21** (1996) 87–93.
11) H. Iwahara, H. Uchida and I. Yamasaki: Int. J. Hydrogen Energy **12** (1987) 73–77.
12) A. Kudo: J. Ceram. Soc. Jpn. **109** (2001) S81–S88.
13) O. M. Skulberg: in Hydrogen Energy System, -Production and Utilization of Hydrogen and Future Aspects, NATO ASI Series Kluwer Academic Publishers **E-Vol.295** (1995) 95–110.
14) M. Amano, C. Nishimura and M. Komaki: Mater. Trans., JIM **31** (1990) 404–408.
15) A. Nakamura, K. Ninomiya and M. Hotta: J. Fuel Soc. Jpn. (Nenryou Kyoukai Shi) **67** (1988) 1038–1051. (in Japanese)
16) R. M. Barrer: Trans. Faraday Soc. **35** (1939) 628–643.
17) S. Miachon and J. A. Dalmon: in Proceedings of 2002 Materials Research Society Fall Meeting (Dec. 2–6, 2002, Boston, USA) 581.
18) N. Itoh, W. C. Xu and K. Haraya: J. Membr. Sci. **66** (1992) 149–155.
19) S. Uemiya, N. Sato, H. Ando, Y. Kude, T. Matsuda and E. Kikuchi: J. Membr. Sci. **56** (1991) 303–313.
20) C. Hsu and R. E. Buxbaum: J. Nucl. Mater. **141–143** (1986) 238–243.
21) C. Nishimura, M. Komaki, S. Hwang and M. Amano: J. Alloy. Compd. **330–332** (2002) 902–906.
22) R. P. Frohmberg, W. J. Barnett and A. R. Troiano: Trans. Amer. Soc. Met. **47** (1955) 892–924.
23) A. Inoue: Mater. Trans., JIM **36** (1995) 866–875.
24) S. Yamaura, M. Hasegawa, H. M. Kimura and A. Inoue: Mater. Trans. **43** (2002) 2543–2547.
25) R. W. Lin and H. H. Johnson: J. Non-cryst. Solid. **51** (1982) 45–56.
26) O. Yoshinari and R. Kirchheim: J. Less-Common Met. **172–174** (1991) 890–898.
27) J. O. Stroem-Olsen, Y. Zhao, D. H. Ryan, Y. Huai and R. W. Cochrane: J. Less-Common Met. **172–174** (1991) 922–927.
28) S. L. I. Chan and C. I. Chiang: J. Alloy. Compd. **253–254** (1997) 370–373.
29) H. Sakaguchi, N. Taniguchi, H. Seri, J. Shiokawa and G. Adachi: J. Appl. Phys. **64**(2) (1988) 888–892.
30) G. Adachi, H. Nagai and J. Shiokawa: J. Less-Common Met. **149** (1989) 185–191.
31) S. Hara, K. Sasaki, N. Itoh, H. M. Kimura, K. Asami and A. Inoue: J. Membr. Sci. **164** (2000) 289–294.
32) S. Hara, N. Hatakeyama, N. Itoh, H. M. Kimura and A. Inoue: Desalination **144** (2002) 115–120.
33) Y. Shimogaki, H. Komiyama, H. Inoue, T. Masmoto and H. Kimura: J. Chem. Soc. Jpn. **58** (1985), 661–664.
34) T. Takahashi, S. Higashi, T. Kai, H. Kimura and T. Masumoto: Catal. Lett. **26** (1994) 401–409.
35) A. Inoue, K. Ohtera, K. Kita and T. Masumoto: Jpn. J. Appl. Phys. **27** (1988) L2248-2251.
36) A. Inoue, T. Zhang and T. Masumoto: Mater. Trans., JIM **30** (1989) 965–972.
37) X. M. Wang and A. Inoue: Mater. Trans., JIM **41** (2000) 539–542.
38) X. M. Wang, I. Yoshii, A. Inoue, Y. H. Kim and I. B. Kim: Mater. Trans., JIM **40** (1999) 1130–1136.
39) A. Inoue, W. Zhang and T. Zhang: Mater. Trans. **43** (2002) 1952–1956.
40) H. M. Kimura, A. Inoue, S. Yamaura, K. Sasamori, M. Nishida, Y. Shimpo and H. Okouchi: Mater. Trans. **44** (2003) 1167–1171.
41) M. Amano, Y. Sasaki, K. Nakamura, C. Nishimura, M. Komaki and M. Shibata: Kinzokuzairyogijutukenkyujo kenkyu houkokusyu (Annual report of National Research Institute for Metals), **11** (1990) 277–287. (in Japanese)